Supplement of The Cryosphere, 17, 3177–3192, 2023
https://doi.org/10.5194/tc-17-3177-2023-supplement
© Author(s) 2023. CC BY 4.0 License.

The Cryosphere Open Access EGU

Supplement of

The Aneto glacier's (Central Pyrenees) evolution from 1981 to 2022: ice loss observed from historic aerial image photogrammetry and remote sensing techniques

Ixeia Vidaller et al.

Correspondence to: Ixeia Vidaller (ixeia@ipe.csic.es)

The copyright of individual parts of the supplement might differ from the article licence.

2.2 In situ Ground Penetrating Radar (GPR), processing and data interpolation

A total of 32 georeferenced radargrams were recorded in a common offset mode, corresponding to a length of 6.8 km and covering almost the entire glacier surface (Figure S1 and Table S1). To determine the distance recorded in each transect, a GPS was connected to the GPR to obtain the data in "time" tuning: the instrument was configured to transmit pulses at constant time intervals. A wheel odometer connected to the device was used for the shielded antenna. In addition, an external wheel odometer was used to estimate, on the one hand, the distance travelled by the RTA obtained by georeferencing and, on the other hand, compare it to the internal wheel odometers of the shielded antennas. The lengths of the radargrams were measured in different ways. The lengths estimated from the coordinates received with the GPS coupled to the instrument and processed by the ReflexW software were found to correspond most closely to the actual length of the transects performed.

2.3 Glacier area outline, point cloud geolocation and glacier thickness loss computation

In this study, ice thickness loss (perpendicular to the glacier surface) was computed using CloudCompare's M3C2 tool. This method was also used in Vidaller et al. (2021) to determine true reduction in ice thickness (no change in ice depth, which is by definition a vertical difference). This method is not the standard one used for comparison of glacier reduction when working over larger areas and with larger glaciers, where vertical changes are normally calculated (Hugonnet et al., 2021).
In order to compute height change values, the local slope of glacier surface was considered to determine the vertical changes as follows:

$$H = \frac{h}{\cos \propto}$$

Where H is the height change value, h is the ice thickness loss (slope-perpendicular) and α is the slope value.

2.4 Correction and accuracy assessment

The values obtained with the external odometer are significantly different (Table S1) from the other two because the displacement on the surface of the external wheel is not uniform (it can slide without moving) and the surface itself is not flat but has grooves and undulations. On the other hand, the distance estimated by Google Earth, although similar to that determined with ReflexW from the coordinates obtained with decoupled GPS, is subject to errors due to the manual marking of the beginning and end of the radargram in the map.
To check the coherence of the thicknesses obtained, a test was carried out at all the intersections between the transects to detect any inconsistencies in the values. These inconsistencies may be due mainly to the fact that in some sections of the radargrams it is difficult to determine exactly the interface between the ice and the rocky bottom.

Supplementary tables:

Table S1: Main characteristics of antenna frequency, orientation and direction: downward (S–N) or upward (N–S) and E–W or W–E.

Radargram	Antenna (MHz)	Orientation	Longitude (m) (ReflexW coordinates)	Longitude (m) (Google Earth)	Longitude (m) (external odometer)
1037	RTA 100	S–N	336	306	320
1038	RTA 100	N–S	272	354	230
1041	RTA 100	N–S	151		134
1042	RTA 100	E–W	153	143	138
1043	RTA 100	S–N	293	281	278
1044	RTA 100	W–E	197	194	173
1045	RTA 100	N–S	48	38	33
1046	RTA 100	W–E	284	271	387
1047	RTA 100	E–W	56	211	47
1052	RTA 100	E–W	161	–	137
1054 (*)	AP 100	S–N	338	283	279 (*)
1059	RTA 100	E–W	294	266	182
1060	RTA 100	W–E	116	112	74
1061	RTA 100	N–S	49	38	38
1062	RTA 100	E–W	1003	997	838
1063	RTA 100	W–E	242	244	220
1067	RTA 100	W–E	625	607	544
1068	RTA 100	S–N	166	176	159
1069	RTA 100	E–W	699	703	595
1070 (*)	AP 500	E–W	34	32	21 (*)
1071 (*)	AP 500	N–S	30	30	25 (*)
1073	RTA 100	N–S	287	249	250
1074	RTA 100	S–N	379	378	363
1075	RTA 100	N–S	36	45	35
1078	RTA 100	N–S	287	250	255
1079	RTA 100	S–N	116	111	129
1090	RTA 100	S–N	281	279	262
1091	RTA 100	W–E	27	34	25
1093	RTA 100	W–E	171	168	154
1094	RTA 100	E–W	168	166	149
1096	RTA 100	E–W	290	294	235

(*) Shielded antenna, distance measured with internal odometer.

Table S2: Intersection points, radargrams implied in the intersection point, and the thickness difference obtained. As can be seen, radargram 1037 was excluded, because the obtained transect is almost identical to the shielded 100 MHz antenna with higher resolution (1054).

Intersections radargrams	Intersection coordinates	Thickness difference (m)
1041/1042	307611.4; 4722878.4	1.7
1042/1054	307561.8; 4722927.2	0.8
1042/1043	307541.8; 4722941.3	3.4
1041/1052	307635.7; 4722957.3	0.3

1052/1054	307588.3; 4722963.7	2
1052/1043	307563.3; 4722979.6	0.3
1043/1046	307563.3; 4722979.6	0.7
1038/1044	307669.4; 4723132.5	0.6
1044/1045	307669.5; 4723132.5	0.5
1043/1044	307640.9; 4723143.4	0
1046/1059	307487.7; 4723195.1	1
1067/1068	307170.2; 4723329.2	2.1
1062/1068	307207.3; 4723380.7	0.3
1062/1079	306973.9; 4723354.8	2.2
1062/1078	306884.9; 4723587.8	2.6
1062/1067	306743.1; 4723643.9	5.3
1062/1074	306743.1; 4723643.9	0.3
1067/1074	306743.1; 4723643.9	5.6
1062/1073	306649.1; 4723697.2	1.2
1062/1063	306518.1; 4723782.6	3.9
1069/1073	306709.9; 4723772.2	1.4
1069/1074	306796.6; 4723710.5	2.1
1074/1096	306903.7; 4723834.5	0
1069/1078	306905.2; 4723641.4	0.3
1078/1096	306971.9; 472378.01	3.3
1069/1079	306995.3; 4723581.4	1.4
1090/1094	307081.8; 4723697.5	0.2
1093/1096	307151.9; 4723775.1	0.1

Table S3: Mean and maximum ice and snow thickness determined from the different velocities considered within the range of temperate ice. Zsmax acronym corresponds to maximum snow thickness, Zimax to the maximum ice thickness, Zsavg to the mean snow thickness and Ziavg to the mean ice thickness for each transect.

Transect	Thickness	Vn=0.2 m/ns; Vh=0,163 m/ns	Vn=0.2 m/ns; Vh=0,168 m/ns	Vn=0.2 m/ns; Vh=0,157 m/ns
1043	Zsmax (m)	5.59	5.59	5.59
	Zimax (m)	11.95	12.32	11.51
	Zsavg (m)	2.92	2.92	2.92
	Ziavg (m)	7.18	7.40	6.92
1062	Zsmax (m)	2.37	2.37	2.37
	Zimax (m)	32.26	33.25	31.07
	Zsavg (m)	1.52	1.52	1.52
	Ziavg (m)	12.80	13.19	12.33
1073	Zsmax (m)	4.53	4.53	4.53
	Zimax (m)	31.35	32.31	30.20
	Zsavg (m)	2.56	2.56	2.56
	Ziavg (m)	20.53	21.16	19.78

Table S4: Details of the errors associated with the orthomosaics produced for this study. The largest error is associated with geometric correction and residual snow cover in 1981. All images were rectified based on 2020 UAV point cloud. Using the same procedure as in

Vidaller et al. (2021), the uncertainty of the glacier outlines was determined as the root of the quadratic sum of four different sources of error and multiplied by the perimeter of the glacier outline, as previously described by Rabatel et al. (2011).

Year	Photo/Image source	Scale/Pixel size	Error due to the pixel size (m)	Error due to the geometric correction (m)	Error in the delineation (m)	Error due to marginal snow cover (m)	Total uncertainty (m)
1981	IGN	0.35 m	0.4	1.27	2	4	2.8
2020	UAV	0.03 m	0.1	0.02	0.2	0.3	0.79
2021	UAV	0.03 m	0.1	0.02	0.2	0.2	0.72
2022	UAV	0.03 m	0.1	0.02	0.2	0	0.57

Table S5: Main characteristics of the Aneto Glacier over the years of the study.

Year		Area 3D (ha/km^2)	Area 2D (ha/km^2)	Glacier front (m a.s.l.)	Area changes since 1981 (%)	Area changes since 1981 (% yr^{-1})
1981		135.7/1.36	115.49/1.15	2,828	–	–
2011		69.3/0.69	62.59/0.63	2,939	−49.0	−1.6
2020	Principal	47.8/0.48	43.97/0.44	3,011	−61.7	−1.6
	Secondary	4.2/0.04	3.82/0.38	3,170		
2021	Principal	46.1/0.46	41.99/0.42	3,014	−63.1	−1.6
	Secondary	3.9/0.04	3.44/0.03	3,170		
2022	Principal	44.6/0.45	38.29/0.38	3,026	−64.7	−1.6
	Secondary	3.52/0.03	2.9/0.03	3,170		

Table S6: Glacier thickness change over the year of the study.

Method of calculation	1981-2022 (m / m yr^{-1})	1981-2011 (m / m yr^{-1})	2011-2022 (m / m yr^{-1})	2020-2021 (m)	2021-2022 (m)
Slope-perpendicular	-30.5 / -0.7	-17.8 / -0.6	-12.6 / -1.1	-1.5	-2.7
Height change	-45.3 / -1.1	-26.5 / -0.9	-18.6 / -1.7	-2.2	-4.8

Supplementary figures:

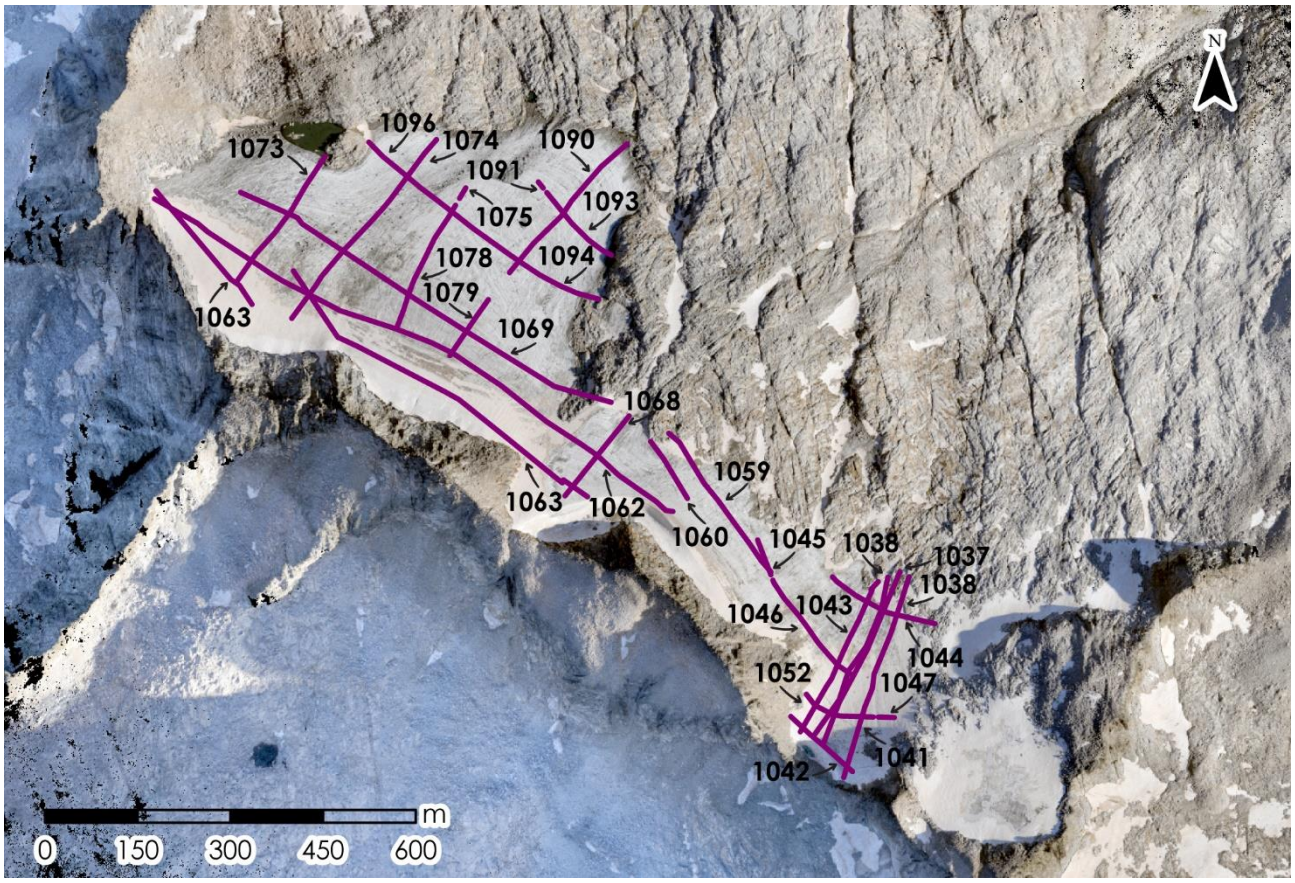

Figure S1: Purple lines indicate radargram transects with their ID number (see the characteristics of each radargram in Table S1).

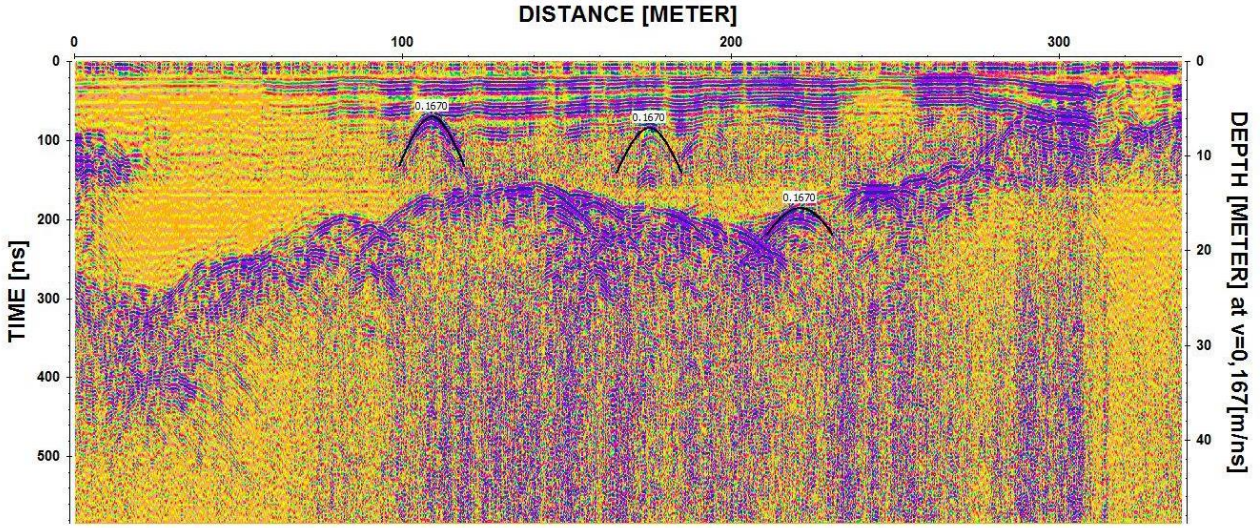

Figure S2: Radargram with the speed obtained in each diffraction hyperbole, considering the established RWV of snow and ice (0,200 and 0,163 m/ns respectively).

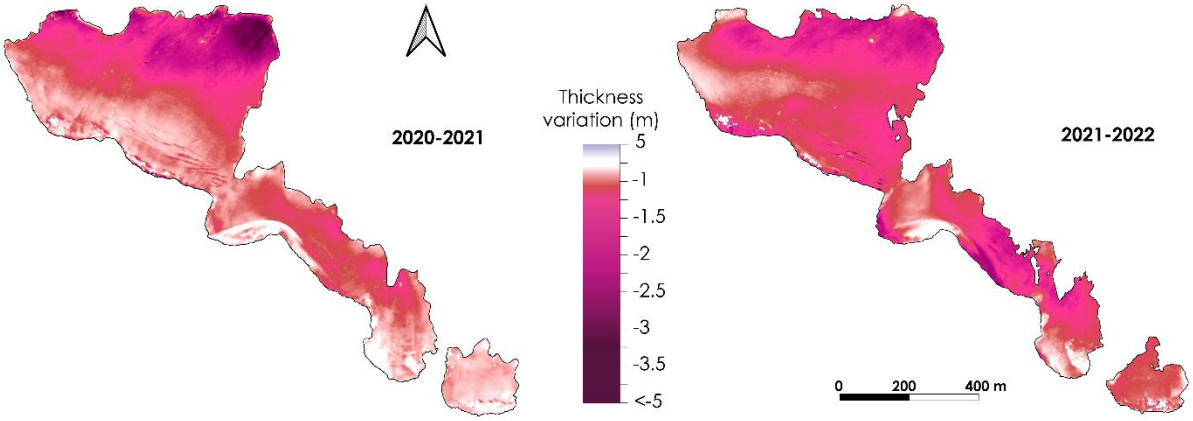

Figure S3: Thickness loss for the periods 2020-2021 (left) and 2021-2022 (right). Data acquired with UAVs surveys. Black arrow determined North direction. The extent of left map corresponds with 2021 Aneto Glacier surface, and the right map with the surface of 2022.

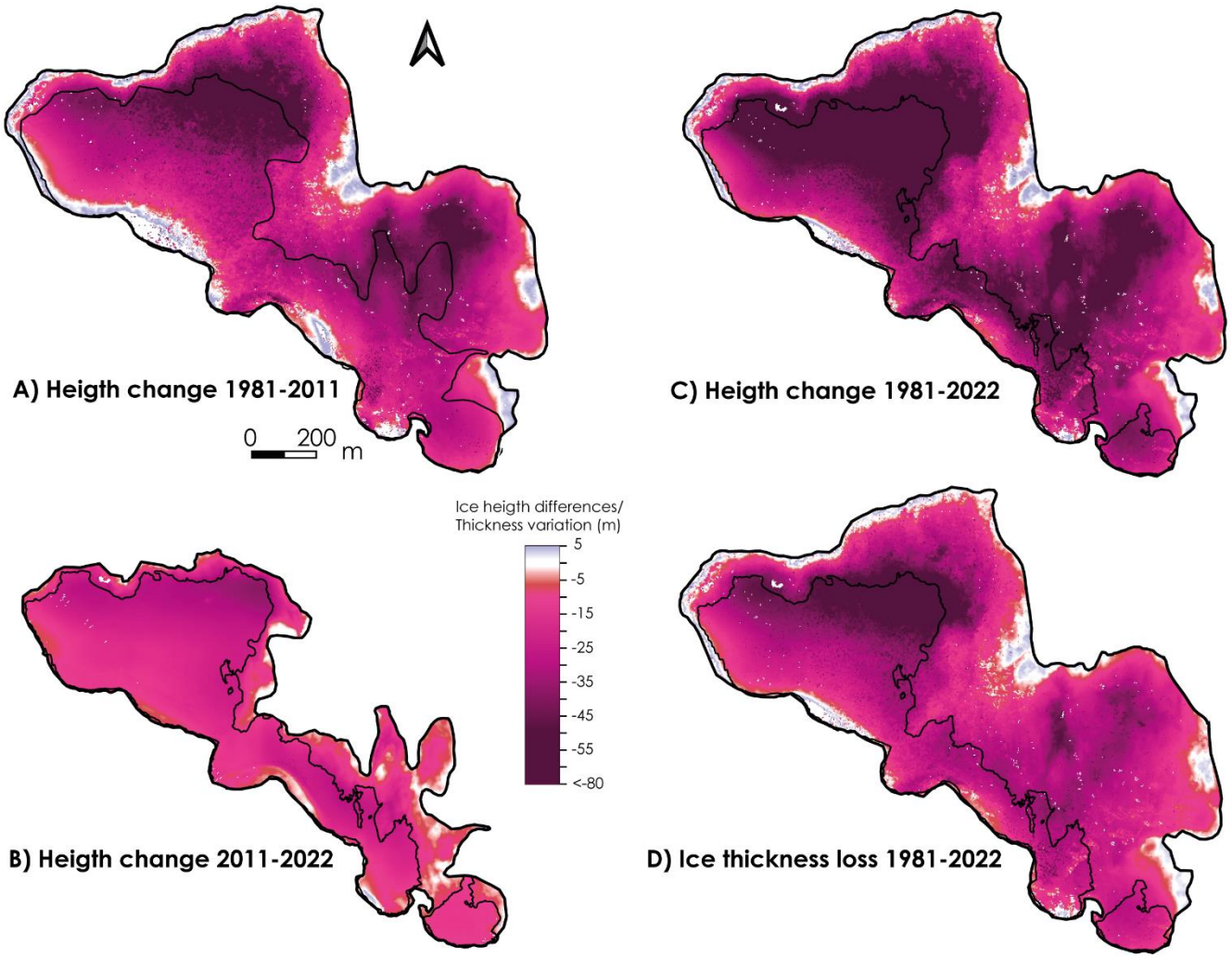

Figure S4: Map A) represents ice height differences (considering differences in the vertical plane) for the period for the period 1981-2011. The thickness (and outer) boundary represents 1981 Aneto Glacier surface, meanwhile the inner black line 2011 Aneto Glacier surface. Map B) shows the ice height differences for the period for the period 2011-2022. The thickness (and outer) boundary represents 2011 Aneto Glacier surface, meanwhile the inner black line 2022 Aneto Glacier surface. Map C) corresponds to ice height differences for the period for the whole period (1981-2022). The thickness (and outer) boundary represents 1981 Aneto Glacier surface, meanwhile the inner black line 2022 Aneto Glacier surface. Map D) represents thickness variation (slope-perpendicular) for the period for the whole period (1981-2022). The thickness (and outer) boundary represents 1981 Aneto Glacier surface, meanwhile the inner black line 2022 Aneto Glacier surface. Black arrow represents North direction. The difference between the two methods show as in this case and due to the small size and high slope, the results of A), B) and C) maps are overestimated.

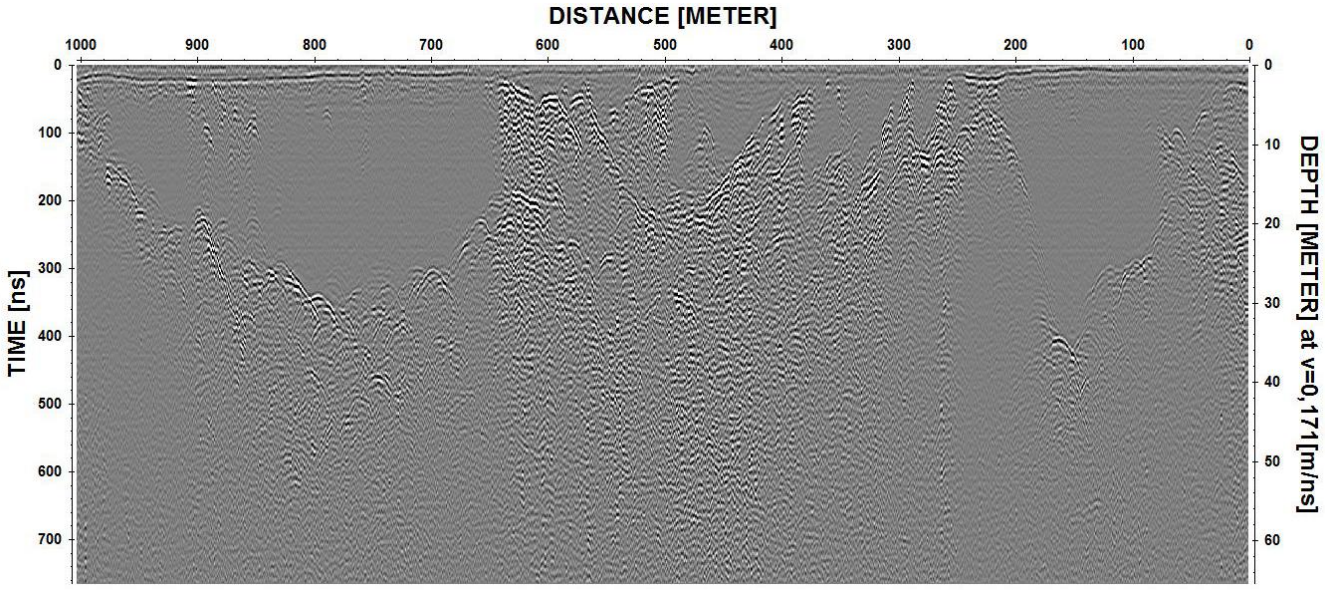

Figure S5: Radargram 1062, representative of the western area. The radargram is represented from SE (0 m) to NW (1000 m), so, from the high part to the lower part of the glacier.

References

Hugonnet, R., McNabb, R., Berthier, E., Menounos, B., Nuth, C., Girod, L., Farinotti, D., Huss, M., Dussaillant, I., Brun, F., and Kääb, A.: Accelerated global glacier mass loss in the early twenty-first century, Nature, 592, https://doi.org/10.1038/s41586-021-03436-z, 2021.

Vidaller, I., Revuelto, J., Izagirre, E., Rojas-Heredia, F., Alonso-González, E., Gascoin, S., René, P., Berthier, E., Rico, I., Moreno, A., Serrano, E., Serreta, A., and López-Moreno, J. I.: Toward an ice-free mountain range: Demise of Pyrenean glaciers during 2011–2020, Geophys Res Lett, 48, https://doi.org/10.1029/2021GL094339, 2021.